How to cite: *Angew. Chem. Int. Ed.* **2022,** *61,* e202205287
International Edition: doi.org/10.1002/anie.202205287
German Edition: doi.org/10.1002/ange.202205287

N-Heterocycles

Oxidative Cyclodehydrogenation of Trinaphthylamine: Selective Formation of a Nitrogen-Centered Polycyclic π-System Comprising 5- and 7-Membered Rings

Johannes Nebauer[+], Christian Neiß[+], Marcel Krug, Alexander Vogel, Dominik Fehn, Shuhei Ozaki, Frank Rominger, Karsten Meyer, Kenji Kamada, Dirk M. Guldi, Andreas Görling, and Milan Kivala**

Abstract: We describe a new type of nitrogen-centered polycyclic scaffold comprising a unique combination of 5-, 6-, and 7-membered rings. The compound is accessible through an intramolecular oxidative cyclodehydrogenation of tri(1-naphthyl)amine. To the best of our knowledge this is the very first example of a direct 3-fold cyclization of a triarylamine under oxidative conditions. The unusual ring fusion motif is confirmed by X-ray crystallography and the impact of cyclization on the electronic and photophysical properties is investigated both experimentally and theoretically based on density-functional theory (DFT) calculations. The formation of the unexpected product is rationalized by detailed mechanistic studies on the DFT level. The results suggest the cyclization to occur under kinetic control via a dicationic mechanism.

Introduction

Within the vigorously developing research on polycyclic aromatic hydrocarbons (PAHs) as defined molecular fragments of sp^2-hybrid carbon allotropes, on the one hand,[1] and innovative organic materials, on the other,[2] nitrogen-containing PAHs represent a particularly appealing compound family.[3,4] In these scaffolds the nitrogen atom with its favorable van der Waals radius readily adopts a trigonal planar geometry upon sp^2 hybridization to provide for efficient delocalization of its lone pair of electrons over the surrounding π system.[4] Thus, without dramatic structural changes, the electronic nature of the entire polycyclic scaffold can be efficiently modified,[5] which opens interesting perspectives for fundamental studies and technological applications.

Since the seminal work of Boekelheide on cyclazines in the 1950s,[6] a variety of PAHs with embedded nitrogen atoms have been realized through specialized synthetic routes. For example, polycyclic azomethine ylides provided access to PAHs of different topologies through 1,3-dipolar cycloadditions and dimerizations followed by intramolecular cyclizations.[7,8] Another synthetic route employed nucleophilic aromatic substitutions between perfluorinated aromatics and pyrrole-based nucleophiles with subsequent oxidative cyclodehydrogenation.[9,10] In addition, on-surface synthesis was established for the fabrication of extended polycyclic architectures selectively doped with nitrogen.[8,11]

[*] Dr. J. Nebauer,[+] A. Vogel, Dr. F. Rominger, Prof. Dr. M. Kivala
Institute of Organic Chemistry, Ruprecht-Karls-Universität Heidelberg, Im Neuenheimer Feld 270, 69120 Heidelberg (Germany)
E-mail: milan.kivala@oci.uni-heidelberg.de
Dr. J. Nebauer,[+] A. Vogel, Prof. Dr. M. Kivala
Centre for Advanced Materials, Ruprecht-Karls-Universität Heidelberg, Im Neuenheimer Feld 225, 69120 Heidelberg (Germany)
Dr. C. Neiß,[+] Prof. Dr. A. Görling
Department of Chemistry and Pharmacy, Chair of Theoretical Chemistry, Friedrich-Alexander-Universität Erlangen-Nürnberg
Egerlandstr. 3, 91058 Erlangen (Germany)
E-mail: christian.neiss@fau.de
M. Krug, Prof. Dr. D. M. Guldi
Department of Chemistry and Pharmacy, Interdisciplinary Center for Molecular Materials (ICMM), Friedrich-Alexander-Universität Erlangen-Nürnberg, Egerlandstr. 3, 91058 Erlangen (Germany)
D. Fehn, Prof. Dr. K. Meyer
Department of Chemistry and Pharmacy, Chair of General and Inorganic Chemistry, Friedrich-Alexander-Universität Erlangen-Nürnberg
Egerlandstr. 1, 91058 Erlangen (Germany)
S. Ozaki, Dr. K. Kamada
Nanomaterials Research Institute (NMRI), National Institute of Advanced Industrial Science and Technology (AIST)
1-8-31 Midorigaoka, Ikeda, Osaka 563-8577 (Japan)
S. Ozaki, Dr. K. Kamada
Department of Chemistry, Graduate School of Science and Technology, Kwansei Gakuin University
Sanda 669-1337 (Japan)
[+] These authors contributed equally to this work.

While these efforts have so far resulted in numerous highly interesting and aesthetically pleasing compounds, the employed synthetic strategies often involve multiple challenging steps and delicate intermediates.[7,12] Hence, an alternative synthetic approach relying on direct cyclization of structurally rather simple triarylamines would be highly desirable. Triarylamines have become ubiquitous as electron-rich constituents of organic functional materials[13] and are readily accessible by transition metal-catalyzed amination protocols.[14]

However, under oxidative conditions, that would be required for the desired cyclization via the Scholl reaction,[15] triphenylamines (TPAs) are known to form highly reactive radical cations which irreversibly dimerize towards benzidines.[16] Back in the 1980s, a direct cyclization of TPAs in the presence of palladium(II) acetate in glacial acetic acid yielding carbazole derivatives was reported.[17] Analogous monocyclizations of TPAs were also achieved photochemically.[18] Recently, partial oxidative cyclizations of arylamines with Ag_2O were reported.[19] In spite of these promising findings, higher cyclizations without preceding *ortho* functionalization of the TPA moiety have yet not been achieved.[20]

Herein, we have developed a modular synthesis of differently substituted tri(1-naphthyl)amines (TNAs) and identified suitable cyclization conditions to achieve an unprecedented nitrogen-centered PAH **1**^{567} comprising 5-, 6-, and 7-membered rings (superscript indices denote the ring-fusion motif around the nitrogen center; Scheme 1). To our surprise, the expected isomeric PAH consisting exclusively of 6-membered rings—denoted in the following as **1**^{666}—was not formed. This is the very first example of a direct 3-fold cyclization of a triarylamine under oxidative Scholl conditions. The unique ring fusion motif was confirmed by single crystal X-ray crystallography and the outcome of the reaction was rationalized by detailed mechanistic studies on the density-functional theory (DFT) level, suggesting the involvement of dicationic intermediates. The impact of planarization on the optoelectronic properties was investigated both in experiment and theory.

Results and Discussion

As the previously reported synthesis of TNA **2** failed in our hands,[21] we developed an alternative route relying on a sequence of Buchwald–Hartwig and Ullmann cross-couplings (see the Supporting Information).[14,22] To investigate the impact of different substituents on the outcome of the oxidative cyclodehydrogenation, we selectively brominated the *para* positions in **2** to achieve compound **3** in 92 % yield (Scheme 1). Subsequent introduction of the 4-(trifluoromethyl)phenyl moieties was achieved by a Suzuki–Miyaura cross-coupling to afford **4** in almost quantitative yield. This chemically robust moiety was chosen to block the reactive *para* positions against intermolecular reactions during subsequent cyclization.[9]

We initially explored the reactivity of compounds **2**–**4** under the standard Scholl conditions using $FeCl_3$ in dry $MeNO_2$ and CH_2Cl_2.[15,23] However, no matter of the temperature and equivalents of the oxidant applied, only partial cyclization accompanied by chlorination leading to complex product mixtures were observed for all compounds. In addition, for TNAs **2** and **3** the formation of dimers and higher oligomers was observed by mass spectrometry (MS). Similar disappointing results, such as no reaction, partial cyclization, decomposition, and dimerization, were obtained for **2**–**4** under alternative conditions using $Pd(OAc)_2$ in glacial AcOH, $Cu(OTf)_2$, and $AlCl_3$ in CS_2, molten $AlCl_3$/NaCl mixture, or upon irradiation by a medium-pressure mercury lamp in different solvents. In contrast, 4-(trifluoromethyl)phenyl-substituted TNA **4** underwent the desired 3-fold cyclization upon treatment with DDQ and trifluoromethanesulfonic acid (TfOH),[24] which was confirmed by high-resolution MS analysis.

We initially envisioned the cyclization to lead to the symmetrical nitrogen-centered PAH **1**^{666} (Scheme 1). However, the ^{1}H and ^{13}C NMR spectra indicated the formation of an unsymmetrical sp^2-carbon framework. Finally, the constitution of the cyclization product was unambiguously elucidated by X-ray diffraction analysis of a single crystal, which was grown by slow evaporation of a CH_2Cl_2/toluene solution at room temperature. The unusual polycyclic framework **1**^{567} exhibits a twisted geometry arising from the fused

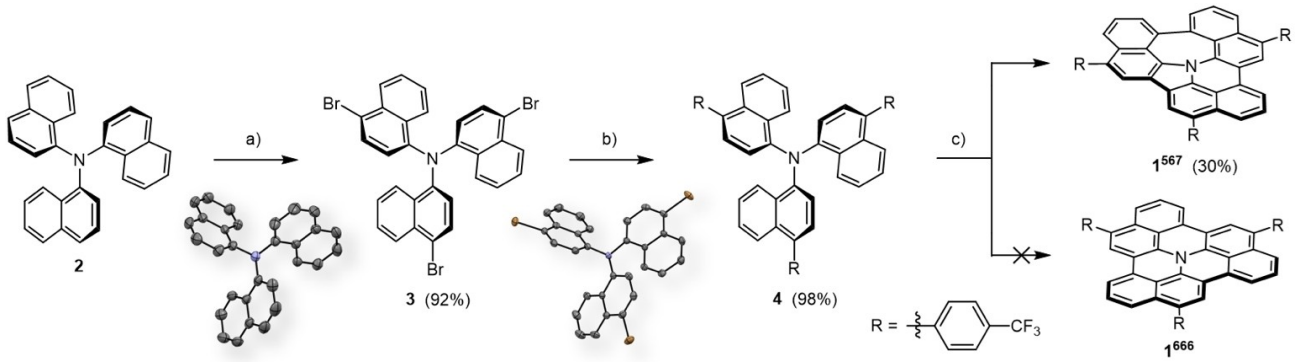

Scheme 1. a) Br_2, CH_2Cl_2, 0 °C, 2 h; b) 4-(trifluoromethyl)phenylboronic acid, $[Pd(PPh_3)_4]$, K_2CO_3, toluene/EtOH 1:2, 100 °C, 23 h; c) DDQ, CF_3SO_3H, CH_2Cl_2, 0 °C to rt, 22 h. X-ray crystal structures of compounds **2** and **3**. DDQ = 2,3-dichloro-5,6-dicyano-*p*-benzoquinone.

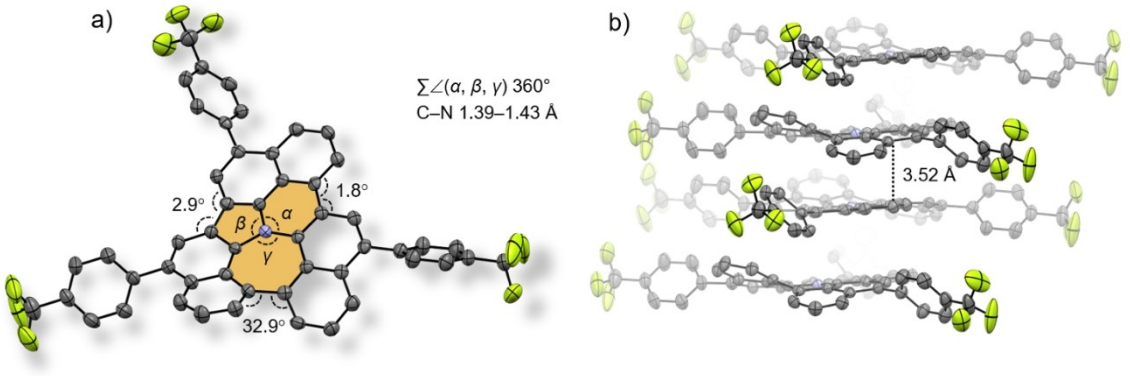

Figure 1. X-ray crystal structure of $\mathbf{1}^{567}$. a) Top view with selected dihedral angles, b) face-to-face columnar arrangement of the individual molecules upon π-π interactions. Selected angles [°]: α (C21–N1–C31) = 134.9(5), β (C21–N1–C11) = 119.5(5), γ (C31–N1–C11) = 105.6(5). H-atoms and solvent molecules omitted for clarity.

5-, 6-, and 7-membered rings (Figure 1a). At closer examination the compound can be regarded as a π-expanded cyclazine with an azaazulene subunit (for the computational assessment of the local (anti)aromaticity, see the Supporting Information).[25] The nitrogen center is planar with the C–N–C angles summing up to 360° and the C–N bond lengths ranging from 1.390(7) to 1.423(7) Å. These features reflect the sp^2-hybridization of the nitrogen center and, thus, its efficient electronic communication with the surrounding π-system. In contrast, the parent TNA features a pyramidalized nitrogen center with Σ_{C-N-C} 348.5° and a C–N_{av} bond length of 1.439(4) Å (see the Supporting Information). In the crystal, $\mathbf{1}^{567}$ adopts a face-to-face columnar arrangement with an average distance of 3.52 Å and the individual molecules being rotated by ca. 60° and slightly slipped with respect to each other. One of the lateral phenyl moieties undergoes edge-to-face C(sp^2)–H···π interactions with the adjacent molecules within the column at a distance of 3.73 Å (Figure 1b).[26] Between the neighboring columns the CF_3 groups are directed towards the hydrogen atoms of the nitrogen-centered framework at distances between 3.31 and 3.40 Å, suggesting weak C(sp^2)–H···F interactions.[27]

To explain the underlying mechanism for the formation of $\mathbf{1}^{567}$, an extensive computational study on the DFT level was carried out (for details, see the Supporting Information). First, the Gibbs free reaction energies of the individual cyclization steps using DDQ were computed (Figure 2). Note that upon each cyclization step, i.e., oxidation, one equivalent DDQ becomes reduced to $DDQH_2$. Compound $\mathbf{1}^{666}$ is more stable than $\mathbf{1}^{567}$ by 19 kcal mol^{-1}, i.e., the experimentally observed formation of $\mathbf{1}^{567}$ results from kinetic and not thermodynamic control of the overall reaction. Because of the high dehydrogenation energies of approximately 35 to 45 kcal mol^{-1} per step, each of these steps is irreversible under the applied reaction conditions, which is in line with the kinetic control of the reaction. Looking at the partially cyclized intermediates we find that the first intermediate $\mathbf{I}^5$ is more stable by 9 kcal mol^{-1} than the intermediate $\mathbf{I}^6$. Throughout, the

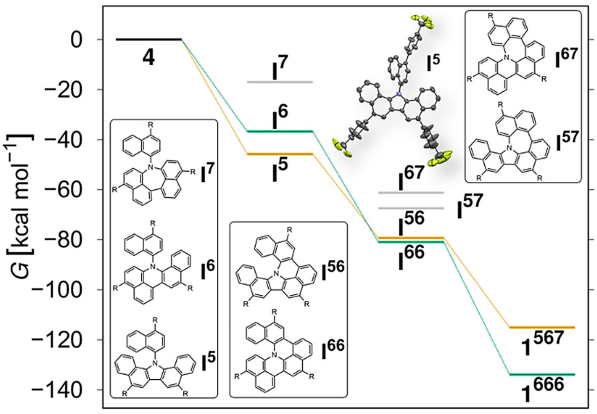

Figure 2. Relative free energies *G* for the stepwise cyclization of **4** with DDQ. The lowest energy path yielding $\mathbf{1}^{567}$ is highlighted in orange, the one yielding $\mathbf{1}^{666}$ in green. The X-ray crystal structure of isolated intermediate $\mathbf{I}^5$ is inserted. R denotes the 4-(trifluoromethyl)phenyl group.

partially cyclized intermediates are denoted as $\mathbf{I}^n$, where n represents the ring sizes formed within the molecule. Species $\mathbf{I}^6$ is destabilized with respect to $\mathbf{I}^5$ due to an unfavorable intramolecular steric interaction (Figure S40).

Since the cyclization steps are irreversible, only $\mathbf{I}^{56}$, $\mathbf{I}^{57}$, and finally $\mathbf{1}^{567}$ can emerge from $\mathbf{I}^5$. Thus, if $\mathbf{I}^5$ is not only more stable than $\mathbf{I}^6$ but also exhibits the lowest activation barrier of formation, the predominant formation of $\mathbf{1}^{567}$ is predetermined. In fact, when the cyclization of **4** was carried out under modified conditions, the postulated monocyclized intermediate $\mathbf{I}^5$ was isolated in 6 % yield (next to $\mathbf{1}^{567}$ (21 %); see the Supporting Information).

As the exact mechanism of the Scholl reaction is hitherto unknown (and may depend on the particular reactants and conditions applied),[15] we considered several possible scenarios. The studies were initially performed for unsubstituted TNA **2** (see the Supporting Information) and subsequently for **4**. We found that the 4-(trifluoromethyl)phenyl groups have no significant effect on

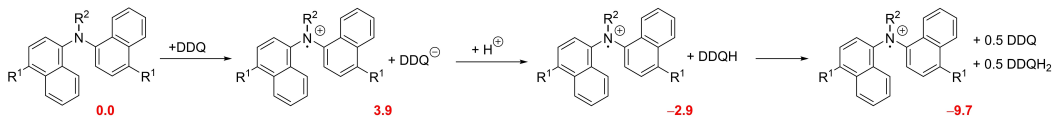

Scheme 2. Oxidation of **4** by a single electron transfer (SET) towards $\mathbf{4}^{\bullet+}$. All ΔG values (red) are relative to **4**, DDQ, and TfOH, and are given in kcal mol^{-1}. Note that "$+H^{\oplus}$" is an abbreviation for "+TfOH, −TfO$^-$".

the intramolecular cyclization, i.e., the electronic effect of these groups is actually quite small, which is in agreement with the experimental data discussed below.

A mechanism starting with the formation of an arenium ion has been suggested for cyclization reactions of oligophenylenes under similar conditions as used in our work.[28] However, the C–C bond formation step is promoted by protonation of rather unfavorable positions of the naphthyl groups like C1 (*ipso*) or C5 (Tables S13 and S14, Schemes S2 and S3). More favorable positions like C2 (*ortho*) and C3 (*meta*) lead to very unstable intermediates and, thus, not to the desired reaction (for details, see the Supporting Information). In the arenium pathway, all transition state energies are quite high (>35 kcal mol^{-1}), and in addition, this mechanism cannot explain why a strong oxidizing agent such as DDQ is needed in the oxidation steps as it seems to be possible using much weaker oxidants.[29]

Another possible mechanism proceeds via radicals generated by a single electron transfer (SET) from TNA to DDQ. As shown in Scheme 2, the initial SET from **4** to DDQ is slightly endergonic by approximately 4 kcal mol^{-1}. In the presence of an acid (in our case TfOH), the DDQ anion becomes protonated, which shifts the equilibrium towards the radical cation $\mathbf{4}^{\bullet+}$. The DDQH radical can be further stabilized as the disproportionation of two DDQH radicals to DDQ and $DDQH_2$ is exergonic by −13.5 kcal mol^{-1}, pushing the equilibrium even further towards $\mathbf{4}^{\bullet+}$. Finally, the radial cation $\mathbf{4}^{\bullet+}$ is favored by nearly 10 kcal mol^{-1} compared to the educts. Note that this process is facilitated only by the protonation of DDQ$^-$, which highlights the crucial role of the acid.

Considering the activation energies needed for the direct cyclization of the radical cation $\mathbf{4}^{\bullet+}$ (Scheme 3), we observe that the transition state energies are lower than in the arenium pathway discussed above. The transition state leading to intermediate $\mathbf{I}^6$ is, however, lower than that of $\mathbf{I}^5$.

Given the high oxidizing power of the DDQ/acid mixture and the fact that we observe two oxidation events in our CV studies of **4** (Table 2), we also took the possibility of generating dications $\mathbf{4}^{2+}$ into account. According to previous studies DDQ/H$^+$ readily oxidizes organic donors up to +1.7 V vs. saturated calomel electrode (SCE).[24,30] The second oxidation potential of **4** occurs at +1.22 V (vs. ferrocene/ferrocenium (Fc/Fc^+) in CH_2Cl_2 with 0.2 M $TBAPF_6$) which corresponds to +1.77 V vs. SCE under analogous conditions.[31] The potential difference of 0.07 V translates to 1.6 kcal mol^{-1} which is in line with our DFT calculations suggesting the formation of $\mathbf{4}^{2+}$ to be endergonic by 1.5 kcal mol^{-1} (Scheme 4). Hence, under the assumption that the electron transfer is not rate limiting, the

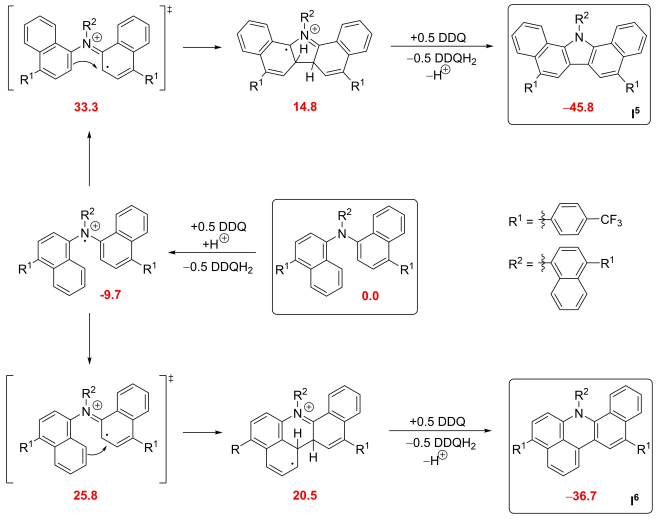

Scheme 3. Radical mechanism via $\mathbf{4}^{\bullet+}$. All ΔG values (red) are relative to **4**, DDQ, and TfOH, and are given in kcal mol^{-1}. Note that "$+H^{\oplus}$" is an abbreviation for "+TfOH, −TfO$^-$", and analogous for "$-H^{\oplus}$".

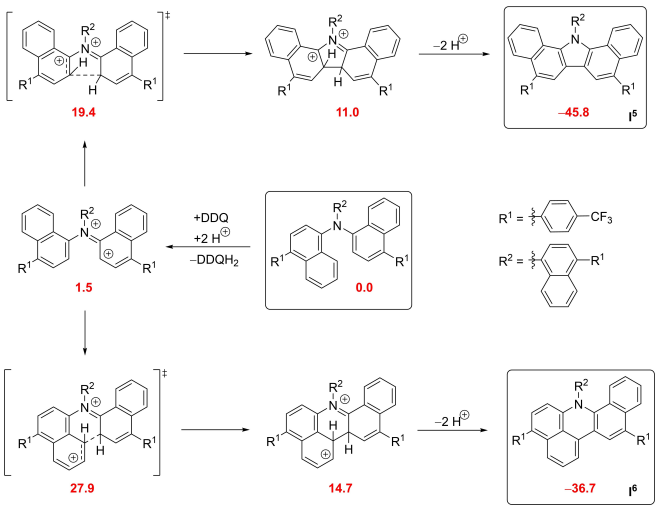

Scheme 4. Dicationic mechanism via $\mathbf{4}^{2+}$. All ΔG values (red) are relative to **4**, DDQ, and TfOH, and are given in kcal mol^{-1}. Note that "$+H^{\oplus}$" is an abbreviation for "+TfOH, −TfO$^-$", and analogous for "$-H^{\oplus}$".

formation of these dications may be considered as a pre-equilibrium to the following cyclization step. Here, the cyclization step yielding intermediate $\mathbf{I}^5$ has the clearly lowest transition state energy of all transition states found (≈20 kcal mol^{-1}). As brought to our attention by one of the

reviewers, a related dicationic mechanism has been proposed recently for cyclizations of a naphthyl-substituted tetracene derivative.[32] The proposed dicationic mechanism also explains why DDQ in the presence of an acid is necessary and why the intermediate **I**[5] forms faster than **I**[6], i.e., under these circumstances the formation of **1**[567] is predetermined.

UV/Vis absorption and fluorescence spectra of **1**[567] and **2**–**4** were measured in CH_2Cl_2 (Figure 3a and Table 1). The introduction of the 4-(trifluoromethyl)phenyl moieties to parent **2** towards **4** results only in a negligible bathochromic shift of 19 nm (0.19 eV) of the longest wavelength absorption. This can be attributed to the limited π-conjugation due to the virtually perpendicular orientation of the electron-poor naphthyl substituents around the nitrogen-centered polycyclic framework. For **1**[567] the lowest energy maximum appears at 406 nm, which corresponds to an additional bathochromic shift of 47 nm (0.40 eV) compared to precursor **4**. The absorption maximum is accompanied by additional low-energy features. The extinction coefficient roughly doubles when going from **4** (31 000 $L\,mol^{-1}\,cm^{-1}$ at 359 nm) to 3-fold cyclized **1**[567] (55 400 $L\,mol^{-1}\,cm^{-1}$ at 327 nm). No solvatochromism was observed for the absorption of **1**[567] and **2**–**4** when going from toluene ($\varepsilon = 2.4$) to chlorobenzene ($\varepsilon = 5.6$), CH_2Cl_2 ($\varepsilon = 8.9$), and benzonitrile ($\varepsilon = 25.2$) (Figure S22 and Table S2).

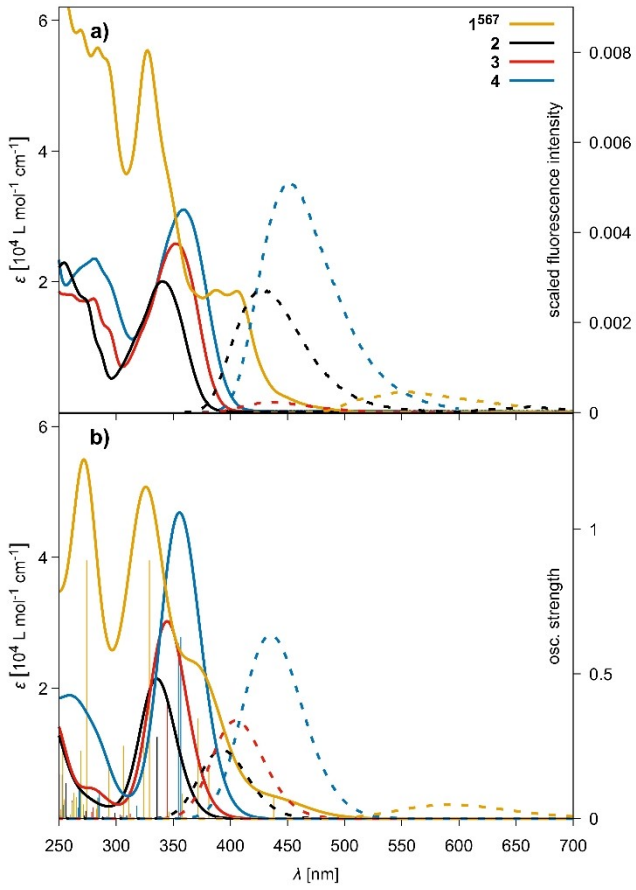

Figure 3. a) Experimental absorption (solid lines) and fluorescence (dashed lines) spectra were recorded in CH_2Cl_2 at room temperature. Excitation wavelength (λ_{exc}) = 410 nm (**1**[567]), 350 nm (**2**–**4**). Fluorescence intensities are normalized such that the integral of the emission band reflects the fluorescence quantum yield (FQY). b) Computed UV/Vis absorption and fluorescence spectra (COSMO-BHLYP/TZVP). In the absorption spectra, the oscillator strengths of the individual electronic excitations are indicated by sticks. As the BHLYP density functional systematically overestimates excitation energies, the theoretical spectra are red-shifted by 0.3 eV for the sake of better comparison. Fluorescence intensities are shown according to their oscillator strengths.

Table 1: Photophysical properties of **1**[567] and **2**–**4**.

Compound	λ_{abs} [nm][a]	ε [$L\,mol^{-1}\,cm^{-1}$]	λ_{em} [nm][a,b]	Φ [%]	τ_F [ns]	$E_{g,opt}$ [eV][c]
1[567]	406	18 500	551	6[d]	14.5	2.66
2	340	20 000	428	21[e]	4.0	3.28
3	352	25 800	438	2[e]	0.2	3.18
4	359	31 000	451	41[e]	3.0	3.09

[a] All spectra recorded in CH_2Cl_2 at room temperature. [b] Excited at the absorption maxima. [c] $E_{g,opt} = h \times c/\lambda_{end}$. [d] vs. Coumarin 153 in EtOH ($\Phi = 0.38$).[34] [e] vs. POPOP in cyclohexane ($\Phi = 0.97$).[35]

To obtain insights into the origin of the absorptions, we conducted time-dependent density-functional theory (TD-DFT) computations (Figure 3b; for further details, see the Supporting Information). The lowest energy absorption maxima of **2**–**4** cover two degenerate excitations from the HOMO to the two degenerate LUMOs, respectively. These are more localized on the peripheral aromatic branches, which increases the dipole moment of the first excited state (for the molecular orbitals of **4**, see Figure S35). The lowest excitation of **1**[567] is rather weak and causes the long tail of the lowest energy absorption band. This excitation corresponds to the HOMO→LUMO transition and is accompanied by a significant charge redistribution, mostly located around the nitrogen-centered cyclazine core. Inspection of the orbitals shows that electron density is transferred from the 5-membered ring (and the adjacent 6-membered rings) to the 7-membered ring (and its adjacent 6-membered rings) (Figure S36). As a consequence, the relatively large dipole moment of **1**[567] (≈5.0 D in solution and ≈4.0 D in the gas phase) originating from the azaazulene moiety drastically reduces in the first excited state (≈0.8 D in the gas phase) and changes its orientation. The first intense absorption band around 400 nm covers two excitations originating from HOMO→LUMO+1 and HOMO→LUMO+2 transitions. Higher excitations are more complex and cannot be easily identified with electronic transitions between single orbitals. For comparison, compound **1**[666] is predicted to display a significantly narrower electronic gap and consequently a pronounced bathochromic shift of the lowest energy absorption occurring at ≈450–500 nm (Figure S39).

When exciting at 350 nm in CH_2Cl_2, **2**–**4** reveal blue fluorescence with maxima at 428, 438, and 451 nm, respectively. The energetic position of the fluorescence maximum strongly depends on the solvent polarity (Figure S22). Going, for example, from non-polar toluene to polar benzonitrile all fluorescence maxima red-shift. This is in line

with the charge transfer in the excited state from the electron rich nitrogen center to the peripheral aromatic branches noted above (Figure S35). After 410 nm excitation in CH_2Cl_2, **1**[567] shows orange fluorescence with a maximum at 551 nm. In stark contrast to **2**–**4**, only a minor solvent dependence is observed, which can be explained by the much smaller and differently oriented dipole moment of **1**[567] in the first singlet excited state compared to its ground state. Thus, the interaction between **1**[567] and the solvent molecules is relatively small in the lowest excited state and a rather small solvent dependency of the fluorescence is expected.[33] Compounds **2** and **4** have fluorescence quantum yields (FQY) of 0.21 and 0.41, respectively, in CH_2Cl_2. Heavy atom effects stemming from the bromo substituents quench the fluorescence of **3** to 0.02. With 0.06 the FQY of **1**[567] is drastically reduced compared to **4**. Assuming that fluorescence occurs from the lowest singlet excited state (Kasha's rule), the relatively low fluorescence quantum yield of **1**[567] compared to **2** and **4**, may be at least in part explained with the lower oscillator strength (i.e., lower allowedness) of the $S_1 \rightarrow S_0$ transition (Figure 3b). The computed Stokes shift of **1**[567] amounts to 0.74 eV $\approx$5900 cm^{-1}.

Two-photon absorption (2PA) spectra were measured in CH_2Cl_2 by the Z-scan method. The resulting spectra shown in Figure 4 are classified by their relative magnitude into two groups (for the simulated spectra, see the Supporting Information). Compounds **1**[567] and **4** give rise to 2PA cross sections ($\sigma^{(2)}$) of 50–70 GM throughout the 530 to 580 nm excitation, while **2** and **3** feature 20 GM or less (1 GM = 10^{-50} cm^4 s photon^{-1} molecule^{-1}). *p*-Phenylene linkers in the former cases govern the electronic communication between the core and the peripheral electron-withdrawing CF_3 functionalities despite the overall twisting. In other words, π-extension enhances $\sigma^{(2)}$. Notably, the 2PA signals were below the detection limit of the measurement set-up except for **1**[567] when exciting at 620 nm or beyond. In the long wavelengths range, that is >580 nm, $\sigma^{(2)}$ of **1**[567] was always lager than that of **4**. Similar to the 1PA spectrum, the 2PA spectrum of **1**[567] exhibits an absorption tail on the low-energy flank, which is not present for **4**.

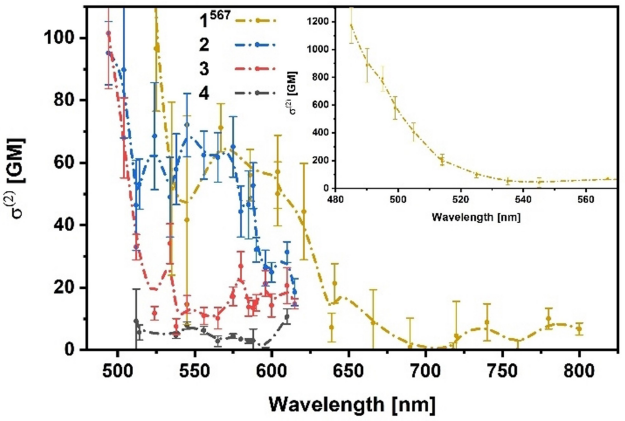

Figure 4. Two-photon absorption cross section ($\sigma^{(2)}$) spectra of **1**[567], **2**, **3**, and **4** in CH_2Cl_2. The inset is that of **1**[567] for shorter excitation wavelengths. The dash-dotted curves are guides to eyes.

Comparing the transition energies of 2PA and one-photon absorption (1PA) indicates that the main 2PA features are energetically closer to higher lying transitions (Figure 4), rather than the lowest-energy transition in the 1PA spectrum. Moreover, **1**[567] and **3** exhibit a drastic amplification of $\sigma^{(2)}$ in the short wavelength range. For **1**[567], $\sigma^{(2)}$ reached 1170 ± 130 GM at 485 nm, despite its overall small molecular size. Considering that the enhancement appears in a wavelength range close to the absorption tail of 1PA it is probably due to resonance enhancement.[36]

Intrigued by the 2PA cross sections, we corroborated the up-conversion in fluorescence assays. Thus, 775 nm laser pulses were used as the off-resonance excitation source. While **2** and **3** failed to yield any appreciable signals, due to their low 2PA cross section at 775 nm, the fluorescence spectra of **1**[567] and **4** are in perfect agreement to the 1PA fluorescence spectra (Figure S24). Furthermore, we verified 2PA by changing the excitation energy from 0 to 80 μJ per pulse. In both cases, the intensity of the fluorescence signal followed a quadratic behavior.[37]

Electrochemical studies of **1**[567] and **2**–**4** together with DFT computations (COSMO-B3LYP/TZVP) provided further insights into their electronic properties (Table 2; for further details, see the Supporting Information). Within the available potential window of CH_2Cl_2 (between ca. −1.25 and +1.50 V vs. Fc/Fc^+) no reduction events were observed, which is in agreement with the computed first reduction potentials occurring below −2.0 V.

All compounds display two oxidation events (except for **2**), TNA **2** is oxidized at +0.78 V (vs. Fc/Fc^+), while unsubstituted TPA is being oxidized at +0.54 V under

Table 2: Electrochemical properties of **1**[567] and **2**–**4**.

Compound	$E_{ox,1}$ [V][a]	$E_{ox,2}$ [V][a]	$E_{ox,1}^{cal}$ [V][b]	$E_{ox,2}^{cal}$ [V][b]	$E_{red,1}^{cal}$ [V][b]	IP_{DPV} [eV][c]	EA_{DPV} [eV][d]	IP^{cal} [eV][b]	EA^{cal} [eV][b]	E_g^{cal} [eV][e]
1[567]	+0.62	+1.15	+0.58	+1.47	−2.13	5.42	2.61	5.18	2.46	2.72
2	+0.78	–	+0.68	+1.65	−2.72	5.54	2.26	5.28	1.88	3.40
3	+0.94	+1.35	+0.84	+1.81	−2.41	5.74	2.58	5.44	2.19	3.25
4	+0.81	+1.22	+0.70	+1.60	−2.37	5.61	2.54	5.29	2.23	3.06

[a] Potentials in V vs. Fc/Fc^+ from differential pulse voltammetry (DPV) in CH_2Cl_2 with 0.2 M $TBAPF_6$. Working electrode: glassy carbon. Counter electrode: Pt. Reference electrode: Ag. [b] Computed potentials referenced to Fc/Fc^+ (COSMO-B3LYP/TZVP; for details, see the Supporting Information). [c] Electrochemical IPs estimated from measured $E_{ox,1}$ and the oxidation potential of soluted Fc against vacuum (4.8 eV).[39] [d] EAs estimated from $E_{g,opt}$ and the respective IP. [e] Electrochemical gaps were calculated as IP^{cal}—EA^{cal}.

analogous conditions.[38] The introduction of the electron-withdrawing bromo moieties in **3** shifts the first oxidation event anodically by 160 mV to +0.94 V. In contrast, the impact of 4-(trifluoromethyl)phenyl acceptors is hardly discernible and compound **4** is oxidized at +0.81 V, which corresponds to an anodic shift of only 30 mV in comparison to parent **2**. This effect is in line with the observations from the UV/Vis absorption spectroscopy and suggests only negligible electronic communication between the lateral acceptors and the nitrogen-centered core in case of **4**. Compound $\mathbf{1}^{567}$ undergoes a facilitated oxidation at +0.62 V, which translates into an anodic shift of 190 mV with respect to precursor **4**. Overall, the calculated electrochemical and ionization potentials (IPs) nicely reproduce the experimentally observed trends (Table 2), with the deviations between the theoretical and experimental data being of systematic nature. The calculated electrochemical gap, i.e., the difference between the adiabatic IP and adiabatic electron affinity (EA) is reduced by 0.36 eV when going from **4** to $\mathbf{1}^{567}$. By combining the CV results with the UV/Vis absorption data (Table 1), the EAs were estimated. According to these data, the HOMO–LUMO gap narrows by 0.26 eV, which nicely corroborates the calculated results.

While the computed potentials for the second oxidation towards the dicationic species reflect the measured trends (Table 2), their values are consistently higher by ≈0.3–0.5 V compared to the experimental ones. This may indicate that the energies of the dicationic species are somewhat overestimated by the dielectric continuum model used in the computations. Such an overestimation may, for example, result from neglecting the increasingly important stabilization of the multiply charged species via ion pairing with the anions of the electrolyte.

Cyclic voltammetry (CV) was utilized to evaluate the reversibility of the oxidations (Figures S19 and S20). The first oxidation is quasi-reversible for **2**–**4** at high scan rates. Spectroelectrochemical studies revealed the irreversible formation of new species upon subsequent transformation of the electrochemically generated radical cations, which is in agreement with the reported behavior of other triarylamines under oxidative conditions.[16] In contrast, the first oxidation of $\mathbf{1}^{567}$ is fully reversible, which indicates considerable stabilization of the electrogenerated radical cation due to efficient charge and spin delocalization within the polycyclic framework. Spectroelectrochemical experiments revealed a broad absorption at 1043 nm and several sharp absorptions at 465, 545, and 664 nm for the radical cation of $\mathbf{1}^{567}$ (Figure S21). The reversibility was confirmed by applying a slightly negative potential. All aforementioned markers of the one-electron oxidized $\mathbf{1}^{567}$ perished, which underlines a sufficient reversibility and stability of the radical cation. The second oxidation is irreversible for all compounds.

Compound $\mathbf{1}^{567}$ was chemically oxidized on a preparative scale with $AgSbF_6$ in CH_2Cl_2 to the corresponding radical cation. The oxidized species was isolated as $[(\mathbf{1}^{567})^{\bullet+}\ SbF_6^-]$ in quantitative yield. The compound forms a dark amorphous solid which was stable for several weeks under ambient conditions exposed to air. According to our DFT computations the molecular orbitals of $(\mathbf{1}^{567})^{\bullet+}$ are quite similar to those of neutral $\mathbf{1}^{567}$ and the electronic structure of the cation is best described as that of $\mathbf{1}^{567}$ with one electron removed from its HOMO. Moreover, the computed spin density nicely resembles the HOMO of $\mathbf{1}^{567}$ (Figure 5a and Figure S36). Electron paramagnetic resonance (EPR) spectra of $(\mathbf{1}^{567})^{\bullet+}$, which were recorded with a 10 μM solution in CH_2Cl_2 at different temperatures ranging from 7 to 293 K (Figure 5b and Figures S25–S30), show an isotropic signal with an effective *g*-value varying from 2.0035 at 7 K to 2.0040 at 293 K. Hyperfine coupling to the ^{14}N nucleus is not observed. This finding indicates a high degree of delocalization, that is, the spin and charge are not exclusively located at the nitrogen center, as already hypothesized from the observed increased stability of $\mathbf{1}^{567}$ during the electrochemical studies. The UV/Vis absorption spectrum in CH_2Cl_2 displays several maxima of low intensity with the lowest

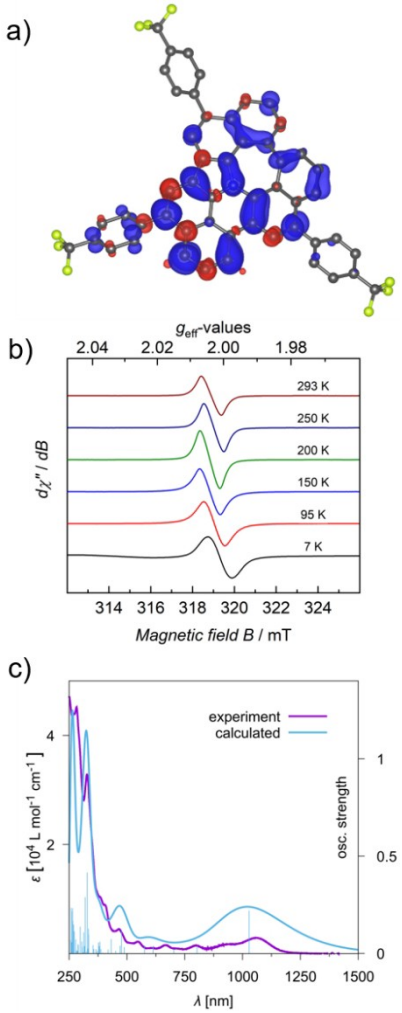

Figure 5. a) Calculated spin density of $(\mathbf{1}^{567})^{\bullet+}$ (COSMO-B3LYP/TZVP), isosurface plotted at 0.001 e Bohr^{-3}. b) Experimental CW X-band EPR spectra of $(\mathbf{1}^{567})^{\bullet+}$ as a 10 μM solution in CH_2Cl_2 at different temperatures. Experimental conditions: microwave frequency $\nu = 8.959$ GHz, modulation amplitude = 1.0 mT, microwave power = 1.0 mW, modulation frequency = 100 kHz, time constant = 0.1 s. c) Experimental and calculated UV/Vis absorption spectra of $(\mathbf{1}^{567})^{\bullet+}$. Experimental and computational details as in Figure 3.

energy absorption occurring at 1057 nm (Figure 5c). The transition to the lowest excited state of $(\mathbf{1}^{567})^{\bullet+}$ (corresponding to the HOMO−1→SOMO transition) reveals a very small oscillator strength and is therefore not visible in the absorption spectrum. The absorption at 1057 nm is due to excitation to the second excited state of $(\mathbf{1}^{567})^{\bullet+}$ and corresponds dominantly to the HOMO−2→SOMO transition in $(\mathbf{1}^{567})^{\bullet+}$.

Conclusion

We have demonstrated for the very first time the ability of substituted tri(1-naphthyl)amine to undergo a 3-fold intramolecular cyclization under oxidative conditions. The cyclization delivered exclusively the unprecedented nitrogen-centered PAH comprising 5-, 6-, and 7-membered rings. The unique ring fusion motif was confirmed by single crystal X-ray crystallography and the product formation was rationalized by extensive mechanistic studies on the DFT level, suggesting the oxidative cyclodehydrogenation to proceed under kinetic control via a dicationic mechanism. The impact of cyclization on the optoelectronic properties was evaluated by UV/Vis absorption and fluorescence spectroscopy as well as comprehensive electrochemical studies. The nitrogen-centered compound displays pronounced two-photon absorption cross sections and forms a persistent radical cation. The experimental results were corroborated by DFT calculations. Our results provide new insights into the mechanistic aspects of oxidative cyclodehydrogenations involving electron-rich substrates and are expected to pave the way towards new families of nitrogen-containing PAHs.

Acknowledgements

The generous funding by the Deutsche Forschungsgemeinschaft (DFG)—Project number 182849149—SFB 953. Dr. Natalie Hammer (Department of Chemistry and Pharmacy, Friedrich-Alexander-Universität Erlangen-Nürnberg) is acknowledged for the initial synthesis of compound **2**. Open Access funding enabled and organized by Projekt DEAL.

Conflict of Interest

The authors declare no conflict of interest.

Data Availability Statement

The data that support the findings of this study are available from the corresponding author upon reasonable request.

Keywords: Dehydrogenation · Density Functional Calculations · Nitrogen Heterocycles · Polycyclic Systems · Reaction Mechanism

[1] a) Y. Segawa, H. Ito, K. Itami, *Nat. Rev. Mater.* **2016**, *1*, 15002; b) S. H. Pun, Q. Miao, *Acc. Chem. Res.* **2018**, *51*, 1630; c) I. R. Márquez, S. Castro-Fernández, A. Millán, A. G. Campaña, *Chem. Commun.* **2018**, *54*, 6705; d) A. Jolly, D. Miao, M. Daigle, J.-F. Morin, *Angew. Chem. Int. Ed.* **2020**, *59*, 4624; *Angew. Chem.* **2020**, *132*, 4652; e) J. Liu, X. Feng, *Angew. Chem. Int. Ed.* **2020**, *59*, 23386; *Angew. Chem.* **2020**, *132*, 23591; f) W. Zeng, J. Wu, *Chem* **2021**, *7*, 358.

[2] a) W. Pisula, X. Feng, K. Müllen, *Chem. Mater.* **2011**, *23*, 554; b) C. Wang, H. Dong, W. Hu, Y. Liu, D. Zhu, *Chem. Rev.* **2012**, *112*, 2208; c) K. Takimiya, I. Osaka, M. Nakano, *Chem. Mater.* **2014**, *26*, 587; d) Q. Miao, *Adv. Mater.* **2014**, *26*, 5541; e) U. H. F. Bunz, *Acc. Chem. Res.* **2015**, *48*, 1676; f) G. Zhang, J. Zhao, P. C. Y. Chow, K. Jiang, J. Zhang, Z. Zhu, J. Zhang, J. Zhang, F. Huang, H. Yan, *Chem. Rev.* **2018**, *118*, 3447.

[3] a) W. Jiang, Y. Li, Z. Wang, *Chem. Soc. Rev.* **2013**, *42*, 6113; b) M. Stępień, E. Gońka, M. Żyła, N. Sprutta, *Chem. Rev.* **2017**, *117*, 3479; c) X.-Y. Wang, X. Yao, A. Narita, K. Müllen, *Acc. Chem. Res.* **2019**, *52*, 2491; d) A. Borissov, Y. K. Maurya, L. Moshniaha, W.-S. Wong, M. Żyła-Karwowska, M. Stępień, *Chem. Rev.* **2022**, *122*, 565.

[4] M. Hirai, N. Tanaka, M. Sakai, S. Yamaguchi, *Chem. Rev.* **2019**, *119*, 8291.

[5] P. O. Dral, M. Kivala, T. Clark, *J. Org. Chem.* **2013**, *78*, 1894.

[6] a) V. Boekelheide, R. J. Windgassen, *J. Am. Chem. Soc.* **1958**, *80*, 2020; b) R. J. Windgassen, W. H. Saunders, V. Boekelheide, *J. Am. Chem. Soc.* **1959**, *81*, 1459; c) W. Flitsch, U. Krämer, *Adv. Heterocycl. Chem.* **1978**, *22*, 321; d) H. Fallah-Bagher-Shaidaei, R. Farkhonde, L. G. Navideh, *Comput. Theor. Chem.* **2011**, *963*, 525; e) A. Skabeev, U. Zschieschang, Y. Zagranyarski, H. Klauk, K. Müllen, C. Li, *Org. Lett.* **2018**, *20*, 1409.

[7] a) R. Berger, A. Giannakopoulos, P. Ravat, M. Wagner, D. Beljonne, X. Feng, K. Müllen, *Angew. Chem. Int. Ed.* **2014**, *53*, 10520; *Angew. Chem.* **2014**, *126*, 10688; b) R. Berger, M. Wagner, X. Feng, K. Müllen, *Chem. Sci.* **2015**, *6*, 436; c) Q.-Q. Li, Y. Hamamoto, G. Kwek, B. Xing, Y. Li, S. Ito, *Angew. Chem. Int. Ed.* **2022**, *61*, e202112638; *Angew. Chem.* **2022**, *134*, e202112638.

[8] X.-Y. Wang, M. Richter, Y. He, J. Björk, A. Riss, R. Rajesh, M. Garnica, F. Hennersdorf, J. J. Weigand, A. Narita, R. Berger, X. Feng, W. Auwärter, J. V. Barth, C.-A. Palma, K. Müllen, *Nat. Commun.* **2017**, *8*, 1948.

[9] M. Takase, V. Enkelmann, D. Sebastiani, M. Baumgarten, K. Müllen, *Angew. Chem. Int. Ed.* **2007**, *46*, 5524; *Angew. Chem.* **2007**, *119*, 5620.

[10] a) H. A. M. Biemans, C. Zhang, P. Smith, H. Kooijman, W. J. J. Smeets, A. L. Spek, E. W. Meijer, *J. Org. Chem.* **1996**, *61*, 9012; b) M. Lazerges, M. Jouini, P. Hapiot, P. Guiriec, P.-C. Lacaze, *J. Phys. Chem. A* **2003**, *107*, 5042; c) M. Takase, T. Narita, W. Fujita, M. S. Asano, T. Nishinaga, H. Benten, K. Yoza, K. Müllen, *J. Am. Chem. Soc.* **2013**, *135*, 8031; d) M. Żyła-Karwowska, H. Zhylitskaya, J. Cybińska, T. Lis, P. J. Chmielewski, M. Stępień, *Angew. Chem. Int. Ed.* **2016**, *55*, 14658; *Angew. Chem.* **2016**, *128*, 14878; e) K. Oki, M. Takase, S. Mori, A. Shiotari, Y. Sugimoto, K. Ohara, T. Okujima, H. Uno, *J. Am. Chem. Soc.* **2018**, *140*, 10430; f) M. Navakouski, H. Zhylitskaya, P. J. Chmielewski, T. Lis, J. Cybińska, M. Stępień, *Angew. Chem. Int. Ed.* **2019**, *58*, 4929; *Angew. Chem.* **2019**, *131*, 4983.

[11] a) M. Matena, T. Riehm, M. Stöhr, T. A. Jung, L. H. Gade, *Angew. Chem. Int. Ed.* **2008**, *47*, 2414; *Angew. Chem.* **2008**, *120*, 2448; b) C. Bronner, S. Stremlau, M. Gille, F. Brauße, A. Haase, S. Hecht, P. Tegeder, *Angew. Chem. Int. Ed.* **2013**, *52*, 4422; *Angew. Chem.* **2013**, *125*, 4518; c) S. Mishra, M. Krzeszewski, C. A. Pignedoli, P. Ruffieux, R. Fasel, D. T. Gryko, *Nat. Commun.* **2018**, *9*, 1714; d) R. Pawlak, X. Liu, S.

Ninova, P. D'Astolfo, C. Drechsel, S. Sangtarash, R. Häner, S. Decurtins, H. Sadeghi, C. J. Lambert, U. Aschauer, S.-X. Liu, E. Meyer, *J. Am. Chem. Soc.* **2020**, *142*, 12568; e) K. Eimre, J. I. Urgel, H. Hayashi, M. Di Giovannantonio, P. Ruffieux, S. Sato, S. Otomo, Y. S. Chan, N. Aratani, D. Passerone, O. Gröning, H. Yamada, R. Fasel, C. A. Pignedoli, *Nat. Commun.* **2022**, *13*, 511.

[12] a) C.-M. Chou, S. Saito, S. Yamaguchi, *Org. Lett.* **2014**, *16*, 2868; b) N. Hammer, T. E. Shubina, J.-P. Gisselbrecht, F. Hampel, M. Kivala, *J. Org. Chem.* **2015**, *80*, 2418.

[13] a) Y. Shirota, H. Kageyama, *Chem. Rev.* **2007**, *107*, 953; b) J. Wang, K. Liu, L. Ma, X. Zhan, *Chem. Rev.* **2016**, *116*, 14675; c) E. Moulin, J. J. Armao IV, N. Giuseppone, *Acc. Chem. Res.* **2019**, *52*, 975.

[14] a) K. Okano, H. Tokuyama, T. Fukuyama, *Chem. Commun.* **2014**, *50*, 13650; b) P. Ruiz-Castillo, S. L. Buchwald, *Chem. Rev.* **2016**, *116*, 12564; c) R. Dorel, C. P. Grugel, A. M. Haydl, *Angew. Chem. Int. Ed.* **2019**, *58*, 17118; *Angew. Chem.* **2019**, *131*, 17276.

[15] a) M. Grzybowski, K. Skonieczny, H. Butenschön, D. T. Gryko, *Angew. Chem. Int. Ed.* **2013**, *52*, 9900; *Angew. Chem.* **2013**, *125*, 10084; b) M. Grzybowski, B. Sadowski, H. Butenschön, D. T. Gryko, *Angew. Chem. Int. Ed.* **2020**, *59*, 2998; *Angew. Chem.* **2020**, *132*, 3020.

[16] a) E. T. Seo, R. F. Nelson, J. M. Fritsch, L. S. Marcoux, D. W. Leedy, R. N. Adams, *J. Am. Chem. Soc.* **1966**, *88*, 3498; b) S. C. Creason, J. Wheeler, R. F. Nelson, *J. Org. Chem.* **1972**, *37*, 4440; c) K. Sreenath, C. V. Suneesh, V. K. R. Kumar, K. R. Gopidas, *J. Org. Chem.* **2008**, *73*, 3245; d) O. Yurchenko, D. Freytag, L. Zur Borg, R. Zentel, J. Heinze, S. Ludwigs, *J. Phys. Chem. B* **2012**, *116*, 30; e) X. Zheng, X. Wang, Y. Qiu, Y. Li, C. Zhou, Y. Sui, Y. Li, J. Ma, X. Wang, *J. Am. Chem. Soc.* **2013**, *135*, 14912.

[17] D. Hellwinkel, T. Kistenmacher, *Liebigs Ann. Chem.* **1989**, 945.

[18] a) M. Zander, W. H. Franke, *Chem. Ber.* **1966**, *99*, 2449; b) W. Carruthers, *Chem. Commun.* **1966**, 272; c) W. Lamm, W. Jugelt, F. Pragst, *J. Prakt. Chem.* **1975**, *317*, 284.

[19] a) C. K. Rank, A. W. Jones, T. Wall, P. Di Martino-Fumo, S. Schröck, M. Gerhards, F. W. Patureau, *Chem. Commun.* **2019**, *55*, 13749; b) L. Moshniaha, M. Żyła-Karwowska, J. Cybińska, P. J. Chmielewski, L. Favereau, M. Stępień, *Beilstein J. Org. Chem.* **2020**, *16*, 895.

[20] a) D. Hellwinkel, *Chem. Ber.* **1971**, *104*, 1001; b) D. Hellwinkel, *Chem. Ber.* **1974**, *107*, 616; c) S. I. Wharton, J. B. Henry, H. McNab, A. R. Mount, *Chem. Eur. J.* **2009**, *15*, 5482; d) J. Lv, Q. Liu, J. Tang, F. Perdih, K. Kranjc, *Tetrahedron Lett.* **2012**, *53*, 5248; e) A. W. Jones, M.-L. Louillat-Habermeyer, F. W. Patureau, *Adv. Synth. Catal.* **2015**, *357*, 945; f) N. Deng, G. Zhang, *Org. Lett.* **2019**, *21*, 5248.

[21] R. B. Bedford, M. Betham, *Tetrahedron Lett.* **2007**, *48*, 8947.

[22] J. E. Field, T. J. Hill, D. Venkataraman, *J. Org. Chem.* **2003**, *68*, 6071.

[23] a) M. Müller, C. Kübel, K. Müllen, *Chem. Eur. J.* **1998**, *4*, 2099; b) A. A. O. Sarhan, C. Bolm, *Chem. Soc. Rev.* **2009**, *38*, 2730; c) T. Horibe, S. Ohmura, K. Ishihara, *J. Am. Chem. Soc.* **2019**, *141*, 1877.

[24] L. Zhai, R. Shukla, R. Rathore, *Org. Lett.* **2009**, *11*, 3474.

[25] a) W. Flitsch, *Adv. Heterocycl. Chem.* **1988**, *43*, 35; b) N. Abe, *Heterocycles* **2018**, *97*, 43.

[26] L. M. Salonen, M. Ellermann, F. Diederich, *Angew. Chem. Int. Ed.* **2011**, *50*, 4808; *Angew. Chem.* **2011**, *123*, 4908.

[27] a) V. R. Thalladi, H.-C. Weiss, D. Bläser, R. Boese, A. Nangia, G. R. Desiraju, *J. Am. Chem. Soc.* **1998**, *120*, 8702; b) J. D. Dunitz, W. B. Schweizer, *Chem. Eur. J.* **2006**, *12*, 6804.

[28] a) P. Rempala, J. Kroulík, B. T. King, *J. Am. Chem. Soc.* **2004**, *126*, 15002; b) P. Rempala, J. Kroulík, B. T. King, *J. Org. Chem.* **2006**, *71*, 5067; c) J. Liu, A. Narita, S. Osella, W. Zhang, D. Schollmeyer, D. Beljonne, X. Feng, K. Müllen, *J. Am. Chem. Soc.* **2016**, *138*, 2602; d) Y. Han, Z. Xue, G. Li, Y. Gu, Y. Ni, S. Dong, C. Chi, *Angew. Chem. Int. Ed.* **2020**, *59*, 9026; *Angew. Chem.* **2020**, *132*, 9111; e) Y. Zou, Y. Han, S. Wu, X. Hou, C. H. E. Chow, J. Wu, *Angew. Chem. Int. Ed.* **2021**, *60*, 17654; *Angew. Chem.* **2021**, *133*, 17795; f) M. Zhao, S. H. Pun, Q. Gong, Q. Miao, *Angew. Chem. Int. Ed.* **2021**, *60*, 24124; *Angew. Chem.* **2021**, *133*, 24326.

[29] L. Zhai, R. Shukla, S. H. Wadumethrige, R. Rathore, *J. Org. Chem.* **2010**, *75*, 4748.

[30] R. Rathore, C. Zhu, S. V. Lindeman, J. K. Kochi, *J. Chem. Soc. Perkin Trans. 2* **2000**, 1837.

[31] The Fc/Fc^+ oxidation potential occurs at $+0.55$ V vs. SCE (in CH_2Cl_2 with 0.2 M $TBAPF_6$): D. Bao, B. Millare, W. Xia, B. G. Steyer, A. A. Gerasimenko, A. Ferreira, A. Contreras, V. I. Vullev, *J. Phys. Chem. A* **2009**, *113*, 1259.

[32] Chaolumen, M. Murata, A. Wakamiya, Y. Murata, *Angew. Chem. Int. Ed.* **2017**, *56*, 5082; *Angew. Chem.* **2017**, *129*, 5164.

[33] a) W. Liptay, *Z. Naturforsch. A* **1965**, *20*, 1441; b) M. F. Nicol, *Appl. Spectrosc. Rev.* **1974**, *8*, 183.

[34] G. A. Reynolds, K. H. Drexhage, *Opt. Commun.* **1975**, *13*, 222.

[35] M. Mardelli, J. Olmsted III, *J. Photochem.* **1977**, *7*, 277.

[36] a) M. Drobizhev, A. Karotki, M. Kruk, N. Zh. Mamardashvili, A. Rebane, *Chem. Phys. Lett.* **2002**, *361*, 504; b) K. Kamada, K. Ohta, Y. Iwase, K. Kondo, *Chem. Phys. Lett.* **2003**, *372*, 386.

[37] M. Drobizhev, Y. Stepanenko, Y. Dzenis, A. Karotki, A. Rebane, P. N. Taylor, H. L. Anderson, *J. Phys. Chem. B* **2005**, *109*, 7223.

[38] a) Z. Fang, R. D. Webster, M. Samoc, Y.-H. Lai, *RSC Adv.* **2013**, *3*, 17914; b) N. Hammer, T. A. Schaub, U. Meinhardt, M. Kivala, *Chem. Rec.* **2015**, *15*, 1119.

[39] J. Pommerehne, H. Vestweber, W. Guss, R. F. Mahrt, H. Bässler, M. Porsch, J. Daub, *Adv. Mater.* **1995**, *7*, 551.

[40] Deposition numbers 1966403 (**2**), 1970341 (**3**), 1966404 (**1^{567}**), and 2159697 (**I^5**) contain the supplementary crystallographic data for this paper. These data are provided free of charge by the joint Cambridge Crystallographic Data Centre and Fachinformationszentrum Karlsruhe Access Structures service.

Manuscript received: April 11, 2022
Accepted manuscript online: July 28, 2022
Version of record online: August 24, 2022